Oxidation-Driven Lithium Uptake in Nickel-Base Alloys – Smoking-Gun Evidence for an Inner Cathode under LWR Conditions

Journal of Nuclear Materials 625 (2026) 156514

Contents lists available at ScienceDirect

Journal of Nuclear Materials

journal homepage: www.elsevier.com/locate/jnucmat

Short communication

Oxidation-Driven Lithium Uptake in Nickel-Base Alloys – Smoking-Gun Evidence for an Inner Cathode under LWR Conditions

Ageo Meier de Andrade [a,*], Christine Geers [a], Jiaxin Chen [a,b], Itai Panas [a]

[a] Department of Chemistry and Chemical Engineering, Chalmers University of Technology, Gothenburg, Sweden
[b] Studsvik Nuclear AB, Sweden

HIGHLIGHTS

- This study demonstrates that the inner-cathode mechanism, previously proposed for protons, also applies to lithium cations.
- The mechanistic investigation reported here addresses lithium enrichment within the inner oxide scale, as documented in the literature.
- Alloy uptake and lithium enrichment are attenuated because the hydrogen evolution pathway is not applicable to lithium, unlike hydrogen.
- Regarding the consequences of enrichment, this work supports further exploration of alternative pH-control buffers for PWR operation.

GRAPHICAL ABSTRACT

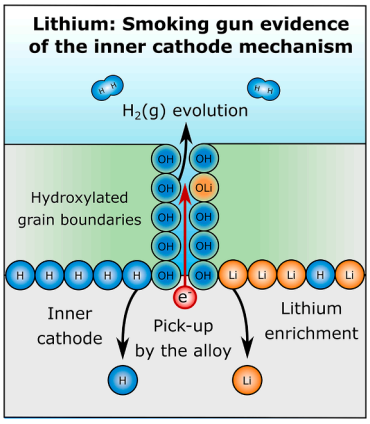

ARTICLE INFO

Keywords:
Inner-cathode mechanism
Lithium uptake
Alloy/oxide interface lithium incorporation
Oxide scale sensitization
Chromia-former Ni-base alloys
Density functional theory

ABSTRACT

Lithium hydroxide is widely used for pH control in pressurized water reactors, yet lithium incorporation in chromia-forming Ni-base alloys has been linked to degraded corrosion resistance. Using lithium as a tracer for protons, we show that Li^+ uptake is consistent with an inner-cathode mechanism for oxidation by water, in which hydroxylated oxide grain boundaries transport molecular water equivalents toward a cathodic region near the alloy/oxide interface. First-principles calculations demonstrate that both H^+ and Li^+ promote chromium oxidation by NiO and catalyse metallic nickel precipitation within the oxide scale, compromising scale integrity. Unlike hydrogen, lithium cannot be removed by molecular evolution and therefore accumulates at the inner cathode. This work provides a mechanistic elucidation of experimentally observed lithium enrichment, which has been suggested to promote stress corrosion cracking in LiOH-containing reactor water.

Nuclear reactor performance is governed by the interplay between load-bearing alloy structure and composition, radiation, and water chemistry [1,2]. Jointly with maintenance, these factors determine the economy of the plant [3].

* Corresponding author.
E-mail address: ageo@chalmers.se (A.M. de Andrade).

https://doi.org/10.1016/j.jnucmat.2026.156514
Received 25 September 2025; Received in revised form 4 February 2026; Accepted 5 February 2026
Available online 6 February 2026

In pressurized water reactors (PWR), alkali hydroxides (MOH) play an important role in controlling the pH under plant operation conditions [4]. The titrant is added to mitigate the corrosive impact of the neutron absorber that is boric acid. In western PWR reactors lithium hydroxide (LiOH) has been widely used, while potassium hydroxide (KOH) has been used for pH control in Water-Water Energetic Reactor (VVER) designs.

Concerns have repeatedly been raised regarding the potential detrimental impact of Li^+ ions [5–10]. Lithium is known to accumulate in the inner (Cr-rich) protective part of the duplex oxide scale that forms on Alloy 690 [11,12]. This is unexpected at first glance since the anode reaction – upon releasing electrons from the alloy/oxide interface to the cathode at the oxide/coolant interface – creates a positive space charge attracting anions while repelling cations, including Li^+.

How can cations, either H^+ or Li^+, overcome the electric barrier and migrate inwards beyond the alloy/oxide interface? In order to resolve this and similar questions one must resort to modelling, be it by means of experiment or theory [13–19].

Our mechanistic understanding emerges from experiment-guided first-principles atomistic modelling. Employing this approach, an analogous paradox was resolved by us in the context of detrimental hydrogen pick-up in zircaloy upon zirconia formation due to oxidation by water [20–22]. More dramatic, the mechanism was generalized to apply in case of inward diffusion of Y^{3+} along oxide grain boundaries during alumina formation on FeCrAl(RE) under low-P_{H_2O} [23–26]. Transient local screening of the instantaneous negative space charge owing to inward diffusion of protons to an "inner" cathode site proximal to the metal/oxide interface is what causes the inward migration of Y^{3+}, and, therefore, formation of yttrium aluminum garnet (YAG) clusters along the alumina grain boundaries (GB) [24]. The cathodic reaction is either hydrogen evolution, hydrogen pick-up, or hydride ions accommodation in oxygen vacancies forming oxy-hydrides [24,27,28]. The complementary reaction at the anode is the newly formed M^{x+} reacting with the surplus O^{2-} from the reduction of the protons, to produce new metal oxide.

This understanding was recently extended to the oxidation of load-bearing chromia forming nickel base alloys by water [29]. A potential cause for hydrogen induced embrittlement in Alloy 690 upon chromia formation was validated, revealing a viable pathway for hydrogen pick-up owing to stress corrosion.

In the three said cases, the reactions are driven by the highly reducing scale former, that is zirconium, aluminum or chromium as facilitated by the corresponding oxide GBs forming hydroxylated oxide interfaces conveying molecular water-equivalents. This offers sustained delivery of oxidizing agents, i.e., H^+, to the reducing "inner" cathode. Proximity to the anode at the receding metal/oxide interface is achieved albeit separated by a thin at times porous barrier oxide, see references [20–22] for Zircaloy. In case of NiO on alloy 690, the essential transformations investigated include H_2(g) evolution, H acting catalyst for the oxidation of Cr by NiO to form Cr_2O_3 and metallic Ni precipitates, and H incorporation in alloy and/or in Ni(s) precipitates [29].

Here, in light of recent experimental observation confirming the accumulation of Li in the inner layer of the oxide scale on Alloy 690 [7, 11,12] and our recent comprehensive mechanistic study of effective water transport in hydroxylated grain boundaries [29], the scope of this work is to explore the viability of Li^+ acting as proton analogue in the water conveyer mechanism for the oxidation of the nickel base chromia former. This work provides a general mechanistic understanding of chemical reactions involving either hydrogen or lithium that are ultimately accumulated at the alloy-oxide interface. We also address key structural differences between the interfaces containing hydrogen and their lithium analogue. We do so by means of first-principles density functional theory, resorting to total energy calculations that include full geometry optimization on lamellar superstructures subject to periodic boundary conditions [29]. Enrichment of lithium presumably results from ppb Li^+/H^+ ion exchange reactions and transport along pathways maintained by the electrochemical inward diffusion of protons. Such exchange reactions between Li^+ and H^+ from hydroxyl groups are common in the synthesis of cathode materials for Li-ion batteries [30] and it has been recently debated in the field of next-generation high--voltage batteries [31]. This work contributes to a general understanding of how Li^+/H^+ ions' reduction is taken to reflect in electrochemical reactions, in particular for the chromium oxidation in load-bearing nickel alloys. Thus, reduced Li^+ either accumulates at the cathode or undergoes pick-up by the metal. Notably, the third pathway corresponding to H_2 evolution is inaccessible for Li. These reactions are summarized in Table 1 and in Fig. 1.

The oxy-hydroxide interface in Fig. 1(a) naturally forms by the hydrolysis at NiO grain boundaries. In the fully lithiated interface shown in Fig. 1(b), lithium tends to occupy nickel sites in the NiO lattice. Experiments reported in the literature also evidence the presence of Li in the vicinity of NiO [7,11,12].

Chromium oxidation (R1) is the most important reaction step of chromia forming functional alloys, where the following steps are conditioned by it. In R1, neighbor oxygen atoms to Li/H are consumed by forming chromia. Somewhat fortuitously, the energetics of Li-O at NiO and its analog comprising H-O at the nickel oxy-hydroxide interface, on acting chromium oxidizing agents, come out almost identical, see Table 1. Indeed, where hydrogen is incorporated in the resulting Ni double-layer, Fig. 1(c), lithium again terminates the NiO grain boundaries, compare Fig. 1(d), and Fig. 1(b).

Two main piggybacking reactions follow:

1. R2a recovers fresh hydroxylated/lithiated interfaces by dissociating from the Ni double-layer, thus readying those for a second chromium oxidation cycle. A book-keeping note is that each such cycle regenerates H^+/Li^+. Thereby, the nominal negative charge associated with oxygen abstraction by Cr, i.e., R1, renders Ni(II) reduced to Ni (0) (see R2a in Table 1). These catalytic cycles are responsible for the precipitation of Ni(s) particles in the oxide scale.
2. R2b incorporates H/Li in the Ni base alloy or Ni precipitates. Both H and Li associate to vacancies $[V_m]@Ni(s)$ to form $\left[V_m^X\right]@Ni(s)$, X = H or X = Li. Thus, the corresponding pick-up processes are controlled by diffusion. A key difference in the pick-up is that hydrogen occupies octahedral interstitial sites in vicinity of a metal vacancy while lithium occupies the metal vacancy site. Also differing is that hydrogen pick-up is slightly endothermic albeit spontaneous because of the $T\Delta S$ term, while lithium pick-up is exothermic by 38 kJ/mol.

For the case of the oxy-hydride interface, a third possible chemical transformation is the hydrogen evolution reaction, R3. Crucially, in case of lithium, such a reaction is not accessible. This, in conjunction with the low metal vacancy diffusivity at reactor operation conditions, is what renders lithium enriched near the alloy/oxide interface, thereby identifying the site where the cathode processes take place. These results offer what can be regarded as smoking..μgun evidence for the inner cathode mechanism for hydrogen.

Our mechanistic understanding of lithium accumulation at the alloy/oxide interface is consistent with recent findings reported by Tsai and co-workers on increased stress corrosion susceptibility caused by lithium incorporation at the alloy/oxide interface in Ni-base alloys [12]. They recently demonstrated that Li^+ ions tend to accumulate at the alloy/-oxide interface in Alloy 600, up to 20 at%, particularly within Cr-rich inner oxide layers and along oxidized metal grain boundaries and showed that lithium promotes the formation of a flaky oxide scale with poor adherence to the alloy matrix. Spectroscopic measurements and Mott–Schottky analysis further revealed that the oxide film becomes thicker when LiOH is used as the pH control agent compared to KOH, and that the higher oxidation rate is accompanied by reduced corrosion resistance. Based on these findings, the authors proposed a mechanism for oxide scale formation in a water medium containing LiOH,

Table 1
Enthalpy of formation (ΔH) per mol X ($X = Li, H$) for the reaction steps in the water conveying mechanism within oxidized grain boundaries of Ni-base alloys. $\Delta\Delta H$ represents the difference in ΔH for each chemical reaction, using as reference the reaction where X = H.

Reaction step	Chemical reaction	ΔH $\left(kJ{\cdot}mol^{-1}\text{ of X atoms}\right)$ X = H	ΔH $\left(kJ{\cdot}mol^{-1}\text{ of X atoms}\right)$ X = Li	$\Delta\Delta H$
R1	$[OX]^{-}Ni(II)[OX]^{-}{\cdot}(NiO)_n + 4/3Cr(s) \rightarrow [X]^{-}Ni(II)[X]^{-}{\cdot}(NiO)_n + 2/3Cr_2O_3$	-103.07	-97.74	+5.33
R2a	$[X]^{-}Ni(II)[X]^{-}(NiO)_2{\cdot}(NiO)_{n-2} + 2[V_m]@Ni(s) \rightarrow [OX]^{-}Ni(II)[OX]^{-}{\cdot}(NiO)_{n-2} + 2\left[V_m^{Ni}\right]@Ni(s)$	-24.98	-30.32	-55.30
R2b	$[X]^{-}Ni(II)[X]^{-}{\cdot}(NiO)_n + 2[V_m]@Ni(s) \rightarrow Ni(0){\cdot}(NiO)_n + 2\left[V_m^{X}\right]@Ni(s)$	+7.72	-37.59	-45.31
R3	$[X]^{-}Ni(II)[X]^{-}{\cdot}(NiO)_n \rightarrow Ni(0){\cdot}(NiO)_n + X_2(g)$	+32.04	—	—

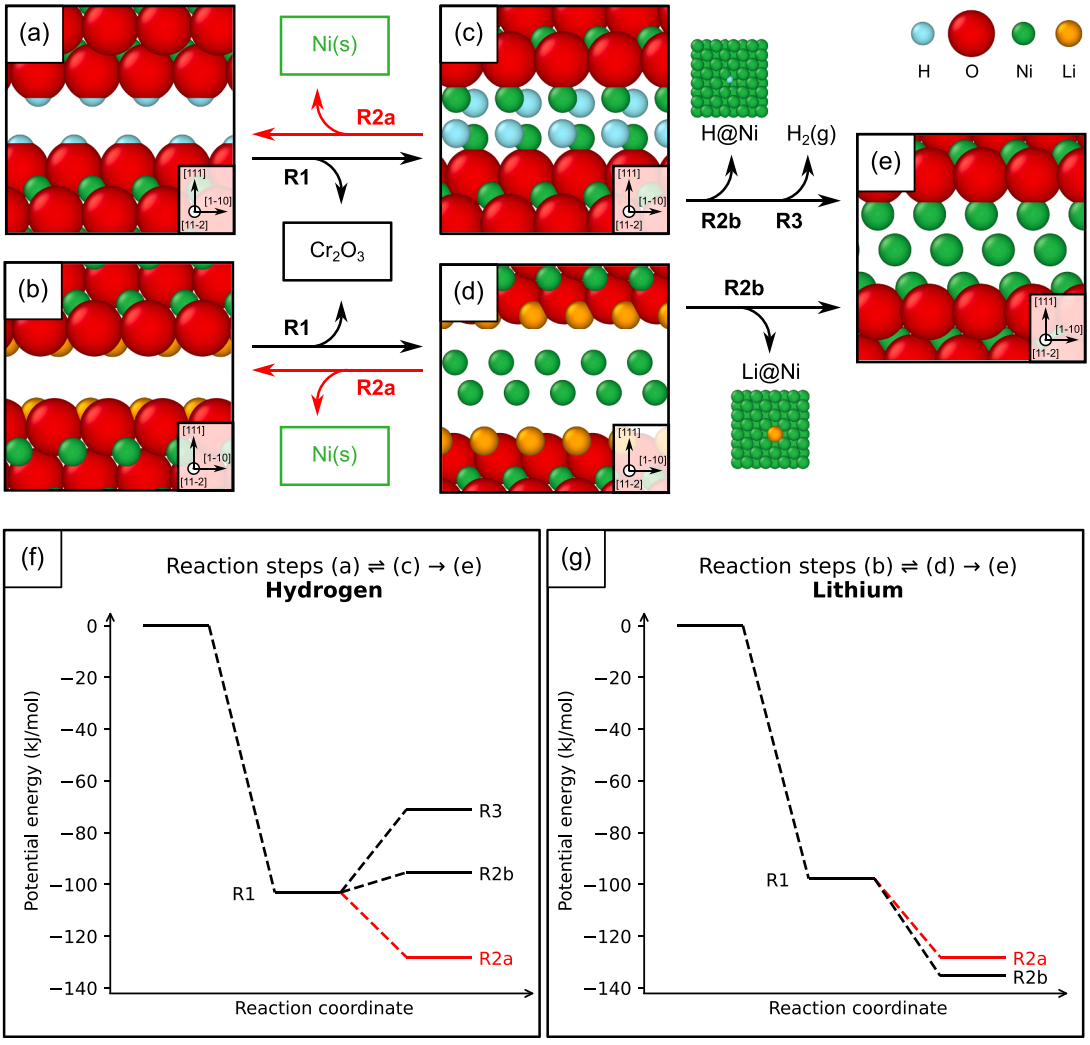

Fig. 1. Panels (a)–(e) show interface models representing oxidized grain boundaries of Ni-base alloys involved in the water-conveying mechanism. Atoms are colored as follows: green for nickel, red for oxygen, light cyan for hydrogen, and orange for lithium. In each panel is indicated the crystal orientation of the NiO lamellae used in the input structure used for atomistic simulations. (a) depicts the oxy-hydroxide interface, and (b) the same interface with H atoms replaced by Li. (c) shows the oxy-hydride interface, and (d) its Li-substituted analogue. (e) represents the oxy-metal interface, which is a product of the chemical transformations R2b, and R3. Panels (f) and (g) show reaction coordinate diagrams, where the y-axis corresponds to the potential energy of the reaction landscape and the x-axis to the reaction coordinate (reaction progress), for interface transformations containing (f) hydrogen (X = H in Table 1) and (g) lithium (X = Li in Table 1).

emphasizing the influence of the hydration enthalpy of Li^{+} ions for its incorporation in the alloy/oxide scale interface. Moreover, in contrast to Li^{+}, experimental studies indicate that K^{+} ions are located primarily in the outer oxide layer, thereby avoiding detrimental enrichment near the alloy/oxide interface [8,12]. In addition to differences in ionic size and solvation behavior, solid-state chemical effects may also play a role — for example, $KFe(III)O_2$ is expected to segregate away from the cathodic region under the prevailing reducing conditions. This would explain why K^{+} ions undergo different diffusion pathways during oxide scale formation under the prevailing conditions.

Here, we highlight the electrochemical oxidation drive causing lithium to accumulate in the inner oxide layers of Alloy 600 by Li^{+} tracking the fate of H^{+} to an inner cathode region in vicinity of the alloy/oxide interface.

In conclusion, a generic mechanistic understanding is offered for the inward transport of cations against the electric field when molecular

water is the sole oxidizing agent. This mechanistic understanding has a strong impact in the field of both nuclear materials and high-voltage battery technology. By emphasising the existence of an inner cathode as conceptual paradigm, when water acts oxidizing agent, this work highlights that, at steady state,

1. Water molecules undergo hydrolysis at outer oxide interfaces to form hydroxide ions that migrate toward an inner cathodic region where protons of hydroxide origin accept electrons from Cr at the alloy/oxide interface, i.e., the anode region; the proton reduction renders the inner cathode negatively charged.
2. Similarly, the resulting Cr^{3+} cations from the electron donation build a positive space charge at the alloy/oxide interface. The build-up of positive and negative space charges is ultimately alleviated by counter-diffusion of metal cations and oxygen anions, which is rate limiting for the scale growth. The negative space charge near the cathode may be intermittently screened by secondary cations from solution, here Li^{+}.
3. Once at the cathode, neither H^{+} nor Li^{+} remain passive spectators but actively participate in electrochemical transformations. The comparative analysis in this work highlights how H^{+} and, to an even greater extent, Li^{+} enrich near the cathode, where they may catalyse the oxidation of chromium by nickel oxide to form particulate metallic nickel precipitates embedded in the oxide. In nuclear power plant operation, this may compromise the protective nature of the barrier oxide, rendering it more susceptible to stress corrosion cracking.
4. In response to stress build-up, the passive layer may develop nano-porosity from strands of oxygen vacancies [21,27], such that either hydrogen or lithium pick-up in the chromia forming alloy may result.
5. In as much as the fates of hydrogen are notoriously difficult to study experimentally, here, lithium serves to track the hydrogen pick-up channel in chromia forming nickel base alloys [12,29].

The generic nature of this electrochemical understanding carries beyond the nickel base chromia formers in load-bearing alloys under LWR conditions. In a recent investigation, motivated partly by the lithium accelerated oxidation kinetics of Zr cladding alloys, Zhang and co-workers report lithium readily diffusing through 2–10 μm thick oxide layers, and further penetrating the metal substrate to several hundred nanometers [32]. The present study explains lithium enrichment by tracking H^{+} to an inner cathode, where it possibly undermines oxide scale integrity. Beyond the alloy/oxide interface and tracing the hydrogen pick-up, lithium ultimately accumulates in point defects within scale forming structural alloys.

1. Modelling considerations

The resilience of load-bearing alloys under aggressive environments is commonly attributed to kinetic control of oxidation. According to the prevailing view, protection arises from the formation of a well-adherent, continuous, and slow-growing barrier oxide that is sustained as well as challenged by this environment. The ideal electrochemical description of this slow growth was originally formulated by Carl Wagner to explain parabolic scale growth and recently it was generalized by us to include the impact of grain boundary density evolution. It involves a cathode at the gas/oxide interface where oxidants are reduced by electron uptake, an anode at the alloy/oxide interface where metal cations are generated, and a growth rate governed by coupled electron and ion transport through the oxide scale.

This “outer-cathode” mechanism typically dominates oxidation in O_2 environments, and also in 100% H_2O environments provided that the oxide exhibits sufficient electronic conductivity. Thus, in both cases, at high temperatures, O^{2-} species are formed through electron transfer: for oxygen, $½O_2 + 2e^- \rightarrow O^{2-}$; for water, $H_2O + 2e^- \rightarrow H_2(g) + O^{2-}$, with protons serving as the oxidizing species in case of the latter.

At intermediate temperatures, the barrier oxide may be short-circuited by low-entropy water-derived species that migrate along hydroxylated interfaces within the oxide scale. These pathways can sustain an “inner-cathode” process near the alloy/oxide interface, thereby facilitating electron transfer from the anode. Although proton reduction remains the cathodic reaction, the constrained environment suppresses hydrogen evolution and enables alternative disposal routes for reaction products. For example, hydride ions may occupy oxygen vacancies [24,27,28] or become absorbed by the underlying alloy [20,22,29].

The resulting complex, heterogeneous oxide morphology—formed through segregation, precipitation, and leaching—is not well suited to rigorous thermodynamic treatment beyond semi-qualitative analysis. Gibbs energy changes tell of spontaneity of the reactions under the relevant conditions. While accurate, these may be misleading as equation of states do not include the time-aspect, i.e the reaction channels accessible on the time scale of the redox- and diffusion processes. Moreover, the change in entropy is commonly subdivided into translational, rotational, and vibrational degrees of freedom. In our study, these contributions are understood to be cancelled as the local coordination of Li on the reactant side and on the product side are very similar. In case of the final step, that is the dissolution of Li in the alloy, however, while being a very slow process, the entropy change is deemed to support this process, i.e., the dissolution into the alloy, which is also observed to take place. Nevertheless, since only parts per billion of lithium is added into the coolant, the overwhelmingly dominant process is the proton reduction that is conditioned by the oxidation process, directing and enriching lithium at the inner cathode.

Thus, cancellation of entropic effects is expected on the time scale of the solid-state mini-processes. Enthalpic stabilities of intermediates along the reaction decide the resulting reactant-intermediate-products trajectory, while $T\Delta S$ is employed as a conceptual framework owing to the said ambiguity in the time-domain. This is exemplified by the formation of H_2 owing to the translational and rotational entropy contributions in the gas phase. The confining environment presented by the inner cathode geometry, however, suppresses the instantaneous translational degrees of freedom, while rotational transform into vibration contributions is not dissimilar to those a priori in the Ni-OH groups prior to the reduction step.

Throughout, we employ first-principles electronic structure calculations to quantify the enthalpy changes of elementary steps as an exploratory approach to identify potentially viable pathways. While viability and mechanistic understanding are central here, activation energies are not considered.

Notably, this methodology is compatible with the experimental reports addressed here concerning Li enrichment near alloy/oxide interfaces and Li uptake into the nickel base alloy. This approach is particularly effective for testing the internal consistency of comprehensive mechanistic frameworks such as the one here, which we have developed previously in our studies.

Our scientific approach rests on a synergistic interplay between experiment and theory: experiments identify phenomena, theory provides model-based interpretation and evaluates the significance of observations, and targeted experiments subsequently refine quantitative understanding once relevance is established. This methodology, subdividing oxidation of metals by water into viable mini-processes has proven robust and productive in the context of corrosion in nuclear materials.

The results reported in this work were obtained by spin-polarised calculations based on density functional theory [33,34] in the implementation with plane waves [35] and pseudopotentials using the CASTEP code [36] within the Materials Studio framework [37]. The Perdew, Burke, and Ernzerhof (PBE) GGA functional [38,39] was employed in all calculations. Core electrons were described by on-the-fly generated norm-conserving pseudopotentials [40], and a plane-wave energy cut-off was set to 1200 eV. The *k*-point sampling of the Brillouin zone was made by means of the Monkhorst-Pack scheme [41,42]

with a *k*-point separation of 0.05 $Å^{-1}$ for all structures. The electronic structure was minimised until the total energy difference was smaller than 10^{-7} eV/atom for two consecutive SCF cycles. A Gaussian smearing scheme with a width of 0.1 eV was used to facilitate convergence. All structures were fully optimised using the L-BFGS [43,44] algorithm with a total energy convergence tolerance of 10^{-5} eV/atom, maximum force tolerance of 0.03 eV/Å, maximum stress tolerance of 0.05 GPa, and maximum displacement tolerance of 10^{-3} Å.

Chemical transformations that take place in oxide scales are implicitly pressurized. Modelling oxide grain boundary interfaces in oxide scales by means of standard DFT calculations should take into consideration the stress field resulting from Pilling-Bedworth expansion while maintaining the adherence to the underlying alloy. Here, a 2 GPa uniaxial external pressure applied normal to the interface results in a 2 Å grains separation. This interface width is stable in the sense that adding pressure only causes increased lateral deformation of the slabs. These values find support in experiments that report 2-3 GPa oxide scale stress [45–48]. Notably, the work to bring the interfaces together is approximately 24 kJ/mol. Indeed, were we to consider free-standing lamella, the first reaction step would be halved, i.e., exothermic by 75 kJ/mol in forming the Ni-H and Ni-Li interfaces. This should be taken to reflect the stresses involved rather than any shortcoming of the model. From a conceptual perspective it tells of the robustness of our emerging understanding. For reference, oxidation of chromium by H_2O(l) and by NiO (s) to form chromia and H_2(g) or Ni(s) is exothermic by 90 kJ/mol and 145 kJ/mol, respectively [49].

CRediT authorship contribution statement

Ageo Meier de Andrade: Writing – review & editing, Writing – original draft, Visualization, Validation, Software, Resources, Project administration, Methodology, Investigation, Funding acquisition, Formal analysis, Data curation, Conceptualization. **Christine Geers:** Writing – review & editing, Writing – original draft, Funding acquisition, Formal analysis, Conceptualization. **Jiaxin Chen:** Writing – review & editing, Writing – original draft, Funding acquisition, Conceptualization. **Itai Panas:** Writing – review & editing, Writing – original draft, Supervision, Resources, Project administration, Methodology, Funding acquisition, Formal analysis, Conceptualization.

Declaration of competing interest

The authors declare that they have no known competing financial interests or personal relationships that could have appeared to influence the work reported in this paper.

Acknowledgments

The authors acknowledge the funding provided by the Swedish Radiation Safety Authority [grant number 2021-7174] and the Swedish Research Council [grant numbers 2018-05973, 2022-06725, 2023-00209]. The computations were enabled by resources provided by the National Academic Infrastructure for Supercomputing in Sweden (NAISS) and the Swedish National Infrastructure for Computing (SNIC) provided by Chalmers e-Commons at Chalmers University of Technology. We also thank David Mayweg for fruitful discussions that helped shape the theoretical perspectives presented in this work.

Data availability

All data generated from the calculations is available at the Swedish National Data repository (SND) and it can be accessed via the following link: https://doi.org/10.71870/ta34-az87.

References

[1] K. Fukuya, Current understanding of radiation-induced degradation in light water reactor structural materials, J. Nucl. Sci. Technol. 50 (2013) 213–254, https://doi.org/10.1080/00223131.2013.772448.
[2] P. Wang, S. Grdanovska, D.M. Bartels, G.S. Was, Corrosion behavior of ferritic FeCrAl alloys in simulated BWR normal water chemistry, J. Nucl. Mater. 545 (2021) 152744, https://doi.org/10.1016/J.JNUCMAT.2020.152744.
[3] S. Uchida, Y. Katsumura, Water chemistry technology – one of the key technologies for safe and reliable nuclear power plant operation, J. Nucl. Sci. Technol. 50 (2013) 346–362, https://doi.org/10.1080/00223131.2013.773171.
[4] A.P. Sorokin, Y.A. Kuzina, R.S. Askhadullin, V.V. Alekseev, Study into the physical chemistry and technology of alkali liquid metal coolants for nuclear and thermonuclear power plants, Nucl. Energy Technol. 9 (1) (2023) 43–49, https://doi.org/10.3897/NUCET.9.101761, 943–49.
[5] A.S. Sinjlawi, L. Dong, M. Ickes, K. Sun, G.S. Was, Irradiation assisted stress corrosion cracking of 347 stainless steel in simulated PWR primary water containing lithium hydroxide or potassium hydroxide, J. Nucl. Mater. 586 (2023) 154676, https://doi.org/10.1016/j.jnucmat.2023.154676.
[6] K. Chen, M.R. Ickes, M.A. Burke, G.S. Was, The effect of potassium hydroxide primary water chemistry on the IASCC behavior of 304 stainless steel, J. Nucl. Mater. 558 (2022) 153323, https://doi.org/10.1016/j.jnucmat.2021.153323.
[7] M. Bojinov, I. Betova, V. Karastoyanov, Corrosion mechanism and electrochemical reactions on Alloy 690 in simulated primary coolant of water–water energy reactors, Materials 17 (2024) 1846, https://doi.org/10.3390/ma17081846.
[8] J. Wang, T. Zhu, Y. Bao, X. Liu, X. Shi, X. Guo, Z. Han, P.L. Andresen, L. Zhang, K. Chen, Insights into the stress corrosion cracking propagation behavior of Alloy 690 and 316 L stainless steel in KOH versus LiOH oxygenated water, Corros. Sci. 224 (2023) 111556, https://doi.org/10.1016/j.corsci.2023.111556.
[9] Y.H. Jeong, J.H. Baek, S.J. Kim, H.G. Kim, H. Ruhmann, Corrosion characteristics and oxide microstructures of Zircaloy-4 in aqueous alkali hydroxide solutions, J. Nucl. Mater. 270 (1999) 322–333, https://doi.org/10.1016/S0022-3115(99)00008-2.
[10] S. Xie, B. Zhou, X. Liang, Q. Li, W. Liu, M. Yao, J. Zhang, The distribution of Li ions in the oxide film formed on zircaloy-4 corroded in lithiated water at 633 K, Materials 13 (2020) 873, https://doi.org/10.3390/ma13040873.
[11] EPRI, Effect of boron concentration on Alloy-690 corrosion product release rates - results at 325°C and 285°C, Palo Alto, CA, 2001.
[12] F.-Y. Tsai, M. Hong, C. Zhou, K.H. Yano, D.K. Schreiber, P. Hosemann, D. Kaoumi, Corrosion sensitivity of nickel-based Alloy Inconel 600 in pressurized water reactor water chemistry: can KOH replace LiOH? Corros. Sci. 255 (2025) 113052 https://doi.org/10.1016/j.corsci.2025.113052.
[13] Z. Gong, X. Wang, L. Li, K. Zhang, S. Yu, J. Li, Z. Cai, Q. He, W. Chou, Z. Shen, Multiscale insights into temperature effects on the sliding wear of a martensitic stainless steel, J. Mater. Res. Technol. 37 (2025) 1174–1185, https://doi.org/10.1016/j.jmrt.2025.06.102.
[14] Y. Zhou, J. Liu, K. Chen, H. Shi, X. Shang, Z. Que, Z. Shen, L. Zhang, X. Zeng, Predicting intergranular stress corrosion cracking of stainless steels in high-temperature water by incorporating crystallographic factor, Acta Mater. 297 (2025) 121322, https://doi.org/10.1016/j.actamat.2025.121322.
[15] Y. Zhou, H. Hu, C. Peng, J. Liu, Y. Zhao, X. Shang, C. Guo, Z. Shen, M. Song, L. Zhang, K. Chen, A precipitation hardened austenitic stainless steel with excellent stress corrosion cracking resistance against high-temperature water, Corros. Sci. 257 (2025) 113352, https://doi.org/10.1016/j.corsci.2025.113352.
[16] J. Li, C. Zhang, K. Zhang, D. Gao, Z. Jiang, Z. Wang, Z. Shen, H. Yang, X. Zeng, Mitigating grain boundary gd segregation to enhance high-temperature oxidation resistance in Mg-6Gd-1Al alloy: a comparative microstructural study, Corros. Sci. 256 (2025) 113256, https://doi.org/10.1016/j.corsci.2025.113256.
[17] K. Chen, Y. Zhou, Y. Zhao, J. Wang, Z. Shen, H. Wang, X. Zeng, Enhancing high-temperature corrosion and cracking resistance of a dual-phase high entropy alloy through surface grinding, Corros. Sci. 256 (2025) 113227, https://doi.org/10.1016/j.corsci.2025.113227.
[18] Q. Xia, D. Hua, Y. Shi, Q. Zhou, B. Zhu, X. Yu, H. Wang, W. Liu, Unveiling the dislocation mechanism induced by irradiation defects in austenitic FeCrNi alloy, Int. J. Plast. 193 (2025) 104451, https://doi.org/10.1016/j.ijplas.2025.104451.
[19] Y. Shi, Q. Xia, M. Xie, Q. Zhou, D. Hua, L. Chai, T. Shi, S.J. Eder, H. Wang, P. Wang, W. Liu, Insights into irradiation-affected structural evolution and mechanical behavior of amorphous carbon, Acta Mater. 281 (2024) 120424, https://doi.org/10.1016/j.actamat.2024.120424.
[20] M. Lindgren, I. Panas, Oxygen vacancy formation, mobility, and hydrogen pick-up during oxidation of zirconium by water, Oxid. Met. 87 (2017) 355–365, https://doi.org/10.1007/s11085-016-9695-z.
[21] M. Lindgren, C. Geers, I. Panas, Possible origin and roles of nano-porosity in ZrO 2 scales for hydrogen pick-up in Zr alloys, J. Nucl. Mater. 492 (2017) 22–31, https://doi.org/10.1016/j.jnucmat.2017.05.017.
[22] M. Lindgren, G. Sundell, I. Panas, L. Hallstadius, M. Thuvander, H.O. Andrén, Toward a Comprehensive Mechanistic Understanding of Hydrogen Uptake in Zirconium Alloys by Combining Atom Probe Analysis With Electronic Structure Calculations, 1543, ASTM Special Technical Publication STP, 2015, pp. 1–25, https://doi.org/10.1520/STP154320120164.
[23] V. Babic, C. Geers, I. Panas, Reactive element effects in high-temperature alloys disentangled, Oxid. Met. 93 (2020) 229–245, https://doi.org/10.1007/s11085-019-09946-6.
[24] V. Babic, C. Geers, B. Jönsson, I. Panas, Fates of hydrogen during alumina growth below yttria nodules in FeCrAl(RE) at low partial pressures of water, Electrocatalysis 8 (2017) 565–576, https://doi.org/10.1007/s12678-017-0368-8.

[25] T. Boll, V. Babic, I. Panas, O. Bäcke, K. Stiller, On aliovalent cations control of α-alumina growth on doped and undoped NiAl, Acta Mater. 210 (2021) 116809, https://doi.org/10.1016/j.actamat.2021.116809.
[26] N. Mortazavi, C. Geers, M. Esmaily, V. Babic, M. Sattari, K. Lindgren, P. Malmberg, B. Jönsson, M. Halvarsson, J.E. Svensson, I. Panas, L.G. Johansson, Interplay of water and reactive elements in oxidation of alumina-forming alloys, Nat. Mater. 17 (2018) 610–617, https://doi.org/10.1038/s41563-018-0105-6.
[27] L. Fine, M. Karlsson, I. Panas, M.M. Koza, Unraveling the electronic control of hydride-ion diffusivity in oxyhydrides from model studies on BaTiO3−2xHx□x, Mater. Adv. 6 (2025) 8885–8893, https://doi.org/10.1039/D5MA00521C.
[28] M. Lindgren, I. Panas, Confinement dependence of electro-catalysts for hydrogen evolution from water splitting, Beilstein J. Nanotechnol. 5 (2014) 195–201, https://doi.org/10.3762/bjnano.5.21.
[29] A.M. de Andrade, C. Geers, J. Chen, I. Panas, Stress-corrosion cracking sensitization by hydrogen upon oxidation of nickel-base alloys by water – an experiment-guided first-principles study, J. Nucl. Mater. 595 (2024) 155044, https://doi.org/10.1016/j.jnucmat.2024.155044.
[30] Y. Sun, J. Pan, P. Wan, X. Liu, The proton exchange chemistry of layered Ni(OH)2 for two types of high-capacity cathode materials in rechargeable batteries, Mater. Res. Bull. 44 (2009) 227–230, https://doi.org/10.1016/j.materresbull.2008.03.013.
[31] G. Wan, T.P. Pollard, L. Ma, M.A. Schroeder, C.-C. Chen, Z. Zhu, Z. Zhang, C.-J. Sun, J. Cai, H.L. Thaman, A. Vailionis, H. Li, S. Kelly, Z. Feng, J. Franklin, S. P. Harvey, Y. Zhang, Y. Du, Z. Chen, C.J. Tassone, H.-G. Steinrück, K. Xu, O. Borodin, M.F. Toney, Solvent-mediated oxide hydrogenation in layered cathodes, Science 385 (2024) 1230–1236, https://doi.org/10.1126/science.adg4687 (1979).
[32] W. Zhang, P.D. Styman, R. Nama, Z. Shah, S. Lozano-Perez, P.A.J. Bagot, M. P. Moody, C.R.M. Grovenor, Lithium penetration to the metal matrix during the in-pile corrosion of Zr cladding alloys, Corros. Sci. 259 (2026) 113472, https://doi.org/10.1016/J.CORSCI.2025.113472.
[33] W. Kohn, L.J. Sham, Self-consistent equations including exchange and correlation effects, Phys. Rev. 140 (1965) A1133–A1138.
[34] P. Hohenberg, W. Kohn, Inhomogeneous electron gas, Phys. Rev. 136 (1964) B864–B871.
[35] M.C. Payne, M.P. Teter, D.C. Allan, T.A. Arias, J.D. Joannopoulos, Iterative minimization techniques for ab initio total-energy calculations - molecular-dynamics and conjugate gradients, Rev. Mod. Phys. 64 (1992) 1045–1097.
[36] S.J. Clark, M.D. Segall, C.J. Pickard, P.J. Hasnip, M.I.J. Probert, K. Refson, M. C. Payne, First principles methods using CASTEP, Zeitschrift Fur Kristallographie 220 (2005) 567–570, https://doi.org/10.1524/zkri.220.5.567.65075.
[37] D.S. BIOVIA, BIOVIA Materials Studio, (2019). https://www.3ds.com/products-services/biovia/resource-center/citations-and-references/(accessed August 5, 2022).
[38] J.P. Perdew, K. Burke, M. Ernzerhof, Generalized gradient approximation made simple, Phys. Rev. Lett. 77 (1996) 3865–3868, https://doi.org/10.1103/PhysRevLett.77.3865.
[39] J.P. Perdew, K. Burke, M. Ernzerhof, Erratum: generalized gradient approximation made simple (physical review letters (1996) 77 (3865)), Phys. Rev. Lett. 78 (1997) 1396, https://doi.org/10.1103/PhysRevLett.78.1396.
[40] D.R. Hamann, M. Schlüter, C. Chiang, Norm-Conserving Pseudopotentials, Phys. Rev. Lett. 43 (1979) 1494, https://doi.org/10.1103/PhysRevLett.43.1494.
[41] H.J. Monkhorst, J.D. Pack, Special points for Brillouin-zone integrations, Phys. Rev. B 13 (1976) 5188–5192.
[42] J.D. Pack, H.J. Monkhorst, "Special points for Brillouin-zone integrations"-a reply, Phys. Rev. B 16 (1977) 1748–1749, https://doi.org/10.1103/PhysRevB.16.1748.
[43] R.H. Byrd, J. Nocedal, R.B. Schnabel, Representations of quasi-Newton matrices and their use in limited memory methods, Math. Prog. 63 (1994) 129–156.
[44] B.G. Pfrommer, M. Cote, S.G. Louie, M.L. Cohen, Relaxation of crystals with the quasi-Newton method, J. Comput. Phys. 131 (1997) 233–240.
[45] G. Calvarin, A.M. Huntz, A. Hugot Le Goff, S. Joiret, M.C. Bernard, Oxide scale stress determination by Raman spectroscopy application to the NiCr/Cr2O3 system and influence of yttrium, Scr. Mater. 38 (1998) 1649–1658, https://doi.org/10.1016/S1359-6462(98)00079-7.
[46] G. Bertali, F. Scenini, M.G. Burke, The effect of residual stress on the preferential intergranular oxidation of Alloy 600, Corros. Sci. 111 (2016) 494–507, https://doi.org/10.1016/j.corsci.2016.05.022.
[47] J. Nychka, Surface oxide cracking associated with oxidation-induced grain boundary sliding in the underlying alloy, Acta Mater. 52 (2004) 1097–1105, https://doi.org/10.1016/j.actamat.2003.10.042.
[48] J. Xiao, N. Prud'homme, N. Li, V. Ji, Influence of humidity on high temperature oxidation of Inconel 600 alloy: oxide layers and residual stress study, Appl. Surf. Sci. 284 (2013) 446–452, https://doi.org/10.1016/j.apsusc.2013.07.117.
[49] S. Zumdahl, Chemical principles, 2009.